International Journal of
Science and Engineering Investigations Vol. 6, issue 70, November 2017
ISSN: 2251-8843

Pipe Deformation Due to Welding

Pham Son Minh[1], Ho Ngoc Son[2]
[1,2]HCMC University of Technology and Education, Vietnam
([1]minhps@hcmute.edu.vn, [2]hongocsonspkt@gmail.com)

Abstract- Welding of two pipes joined by a connector is investigated numerically and experimentally. The simulation is performed in ANSYS finite-element software using its heat-transfer and structural capabilities. To verify the simulation results, a series of experiments is conducted with four different pipe thicknesses using an automated welding process, AISI 1005 low-carbon steel as the parent metal, a gas metal arc welding (GMAW) digital power source with premixed shielding gas, and a one-sided clamping technique. Comparing the simulation and experimental results shows that three-dimensional thermo-elastic-plastic finite-element analysis can predict welding deformation. The simulation results also show that the stress distribution is located on the connector part, which experiences high temperatures in the welding process. However, as the pipe thickness is increased, the deformation becomes less because of lower residual stress.

Keywords- *Welding Simulation, Structure Deformation, Heat Transfer, Pipe Connection, Pipe Deformation*

I. INTRODUCTION

The main problem with welding a metal structure is that the process always leaves some residual stress and deformation. Novice welders (and even some who are more experienced) tend to struggle with the problem of weld deformation (WD), which is warping of the base metal caused by heat from the welding arc. This deformation is troublesome for a number of reasons, but one of the most critical is the potential creation of a weld that is not structurally sound. Most WD results from the expansion and contraction of the weld metal and adjacent base metal during the heating and cooling cycle of the welding process. Welding on one side only of a part will cause far more distortion than if the welds are alternated from side to side. During this heating and cooling cycle, many factors affect how the metal shrinks and possibly distorts, such as those physical and mechanical properties that change as heat is applied. In turn, these changes affect how the heat flows and how uniformly it is distributed.

Because it is impossible to obtain experimental data for every situation, computer simulations of welding are needed to predict the impact of different design options on residual stress and deformation. Finite-element modeling (FEM) has become a useful technique for predicting WD. However, although structural deformation can now be predicted accurately by numerical means, it remains difficult to model welding with FEM. Because of the intense concentration of heat in the welding heat source, regions near the weld line are subject to all manner of boundary conditions (e.g., clamping force, heat transfer, and heating source). Therefore, predicting three-dimensional (3D) WD is of major interest with regard to welding a variety of engineering alloys.

Given recent developments in computing capabilities, it is now feasible and practical to predict residual stresses by full 3D simulation of the arc-welding process. There have been many studies of the thermal distributions and residual stresses due to welding. Zhang et al. [1] used FEM to study the welding process of an automotive gear-case assembly dur automotive gear-case assembly. In this research, the adaptive mesh refinements are used to transfer the results between different meshes [2]. For the analyzing, the thermo-mechanical model used as well as the simulation methodology was detailed. After running, the computed distortions and residual stresses were compared with experimental measurements. Butt welding of stainless steel pipes has been the subject of nonlinear thermo-mechanical FEM [3]. In particular, the axial and hoop stresses and their sensitivity to variation in the weld parameters were studied. In addition, various studies have used combined analytical and experimental methods to analyze the residual stresses in pipes formed with girth butt welds [4–8].

In the present paper, we investigate numerically and experimentally welding of two pipes joined by a connector. The simulation was performed in ANSYS FEM software using its heat-transfer and structural capabilities. To verify the simulation results, we conducted a series of experiments with four different pipe thicknesses using an automated welding process, AISI 1005 low-carbon steel as the parent metal, a gas metal arc welding (GMAW) digital power source with premixed shielding gas, and a one-sided clamping technique. Comparing the simulation and experimental results shows that 3D thermo-elastic-plastic FEM can predict WD.

II. SIMULATION AND EXPERIMENT

We consider the deformation of two pipes welded together with a connector. In both the simulation and the experiment, we used pipes that were 2.5, 3.2, 4.0, and 5.2 mm thick. In the simulation, the material parameters were those listed in Table 1, which are the same as those of the AISI 1005 steel used in

the experiment. In addition, to analyze the heat transfer and deformation of the pipes, we used the material parameters listed in Table 2 in the simulation software.

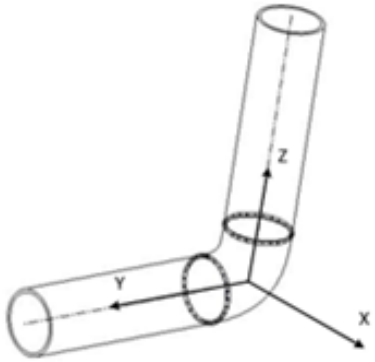

Figure 1. Simulation model

We began the simulation by setting the values of the relevant welding parameters (see Table 3) according to American Welding Standards - AWS. For each pipe thickness, we built a computer-aided design model as shown in Fig. 1. We exported this model to ANSYS in Initial Graphics Exchange Specification (IGES) format, whereupon it was converted into a meshing model with a proper mesh. To improve simulation accuracy while managing the time it took, the mesh was refined locally at the welding area. The evolution thermal analysis is quite a complex phenomenon associated with GMAW. The weld metal transfer mode and corresponding fluid flow dynamics have a large influence on the shape of the weld pool [9]. When applying FEM to GMAW, the double-heat-source model used most is that of Goldak et al. [9] as shown in Fig. 2; the relevant parameter values used herein are listed in Table 4. The meshing model combined with the welding parameters was then sent to the ANSYS solving module to analyze the welding process in relation to the temperature distribution, deformation, and residual stress of the entire welded structure.

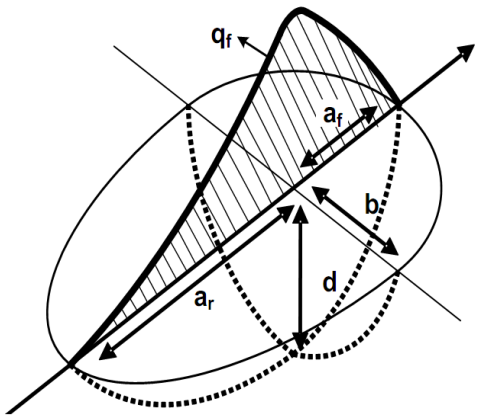

Figure 2. Heat transfer at the welding pool: the Goldak model [9].

TABLE I. CHEMICAL CONTENT OF LOW-CARBON STEEL

Standard	AISI 1005
% C	0.14−0.22
% Si	0.12−0.30
% Mn	0.40−0.65

Figure 3. Material properties of the welding pipe

Material properties	Values
Young Modulus (Gpa)	210 (at 20oC)
Minimum yield strength (Mpa)	355
Poisson's ratio	0.33
Solidus temperature (^oC)	1404
Liquid temperature (^oC)	1505

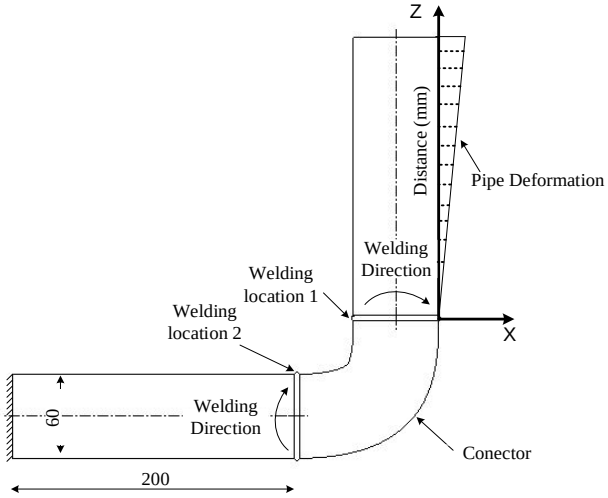

Figure 4. Location for observing welding deformation.

To simulate the welding process and to predict the welding distortion of pipes of differing thickness, we used the linear elastic shrinkage method using relatively new FEM software developed by ANSYS. For verification purposes, we also performed a series of experiments using a fully automated welding system with a GMAW power source. The shielding gas for the welding process was carbon dioxide (CO2). We used a coordinate measuring machine to measure the initial and final dimensions of the specimen. The welding parameters used during the experiments are those listed in Table 3. To assess the influence of pipe thickness on the deformation of the structure, we used pipes of four different thicknesses in the simulation and experiment. The welding process was as follows. First, the two pipes and the connector were joined by point welds. Welding was then conducted at locations 1 and 2 as shown in Fig. 3. Having been welded, the part was left to cool down to room temperature, whereupon we measured the deformation with distance along the Z-axis as shown in Fig. 3. For each pipe thickness, we operated the welding process with 10 parts and then calculated the average deformation for discussion and comparison with the simulation.

III. RESULTS AND DISCUSSION

We consider the pipe deformation along the Z-axis (Fig. 3). The results are collated and compared in Figs. 4 and 5. From these results, it is clear that the thinner pipes (2.5 and 3.0 mm thick) deformed more than did the thicker ones (4.0 and 5.2 mm thick). In addition, the maximum pipe deformation occurred farthest from the welding area. This show that the pipe connection between two pipes with the connector should have the solution for reducing the deformation of the pipe due to the disadvantage of the pipe deformation at the far area of pipe, which will have another connection with another part. According to the simulation results, with a pipe length of 200 mm and the welding structure as in Fig. 3, the maximum deformations are 4.78, 2.68, 1.56, and 1.39 mm for pipe thicknesses of 2.5, 3.2, 4.0, and 5.2 mm, respectively.

By contrast, the highest stress is located at the welding area and in the connector. This indicates that the weak point is close to the connector, which is where the highest temperatures occur in the welding process. Hence, this location requires a higher safety margin compared with other locations. A common and efficient way to reduce the residual stress when welding thinner pipes is to reduce the welding current. This method could also decrease the deformation because the heat transfer to the welding pool would be lower. However, welding quality would suffer if the current was too low. The simulation also shows the influence of pipe thickness on residual stress when welding was operated with the same parameters as in Table 3. When the pipe thickness is increased from 2.5 to 5.2 mm, the maximum residual stress decreased from 402 to 202 MPa.

TABLE II. WELDING PARAMETERS USED FOR THE SIMULATION AND EXPERIMENT

Welding parameters	Unit	Value
Current	A	90
Voltage	V	80
Welding speed	mm/s	3.2

TABLE III. PARAMETERS OF THE GOLDAK DOUBLE-ELLIPSOIDAL MODEL

Parameters of Goldak's double ellipsoid	
af (mm)	4
ar (mm)	7
b (mm)	3.5
d(mm)	3

TABLE IV. SIMULATION AND EXPERIMENTAL RESULTS (PIPE THICKNESS = 2.5 MM)

Distance	10	20	30	40	50	60	70	80	90	100	110	120	130	140	150	160	170	180	190	200
Experiment	1.08	1.25	1.51	1.73	1.96	2.18	2.32	2.5	2.68	2.82	3.21	3.32	3.43	3.65	3.72	3.8	3.94	4.15	4.28	4.5
Simulation	1.14	1.19	1.32	1.47	1.78	2.16	2.38	2.45	2.63	2.77	3.12	3.45	3.53	3.72	3.82	4.05	4.19	4.32	4.54	3.53

TABLE V. SIMULATION AND EXPERIMENTAL RESULTS (PIPE THICKNESS = 3.2 MM)

Distance	10	20	30	40	50	60	70	80	90	100	110	120	130	140	150	160	170	180	190	200
Experiment	0.72	0.78	0.87	0.96	1.05	1.13	1.24	1.35	1.42	1.53	1.62	1.68	1.75	1.86	1.97	2.12	2.18	2.34	2.52	2.61
Simulation	0.77	0.84	1.01	1.22	1.34	1.37	1.46	1.58	1.7	1.75	1.87	1.96	2.08	2.13	2.22	2.3	2.47	2.52	2.62	2.68

TABLE VI. SIMULATION AND EXPERIMENTAL RESULTS (PIPE THICKNESS = 4.0 MM)

Distance	10	20	30	40	50	60	70	80	90	100	110	120	130	140	150	160	170	180	190	200
Experiment	0.42	0.47	0.49	0.53	0.58	0.62	0.68	0.75	0.79	0.87	0.95	1.02	1.06	1.08	1.13	1.22	1.31	1.38	1.43	1.5
Simulation	0.34	0.48	0.54	0.6	0.74	0.82	0.87	0.92	0.98	1.02	1.09	1.11	1.15	1.17	1.21	1.35	1.38	1.42	1.45	1.56

TABLE VII. SIMULATION AND EXPERIMENTAL RESULTS (PIPE THICKNESS = 5.2 MM)

Distance	10	20	30	40	50	60	70	80	90	100	110	120	130	140	150	160	170	180	190	200
Experiment	0.34	0.36	0.38	0.43	0.46	0.51	0.52	0.57	0.65	0.68	0.72	0.78	0.82	0.85	0.87	0.92	0.95	0.98	1.05	1.1
Simulation	0.31	0.36	0.41	0.45	0.48	0.55	0.62	0.67	0.78	0.85	0.87	0.92	0.97	1.02	1.05	1.15	1.18	1.25	1.32	1.39

Form	Temperature (°C)	Deformation (mm)	Residual stress (MPa)
2.5 mm	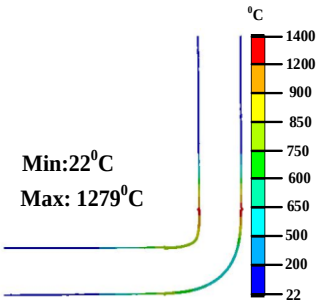	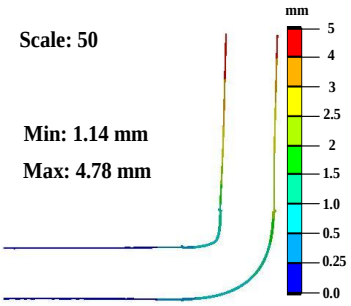	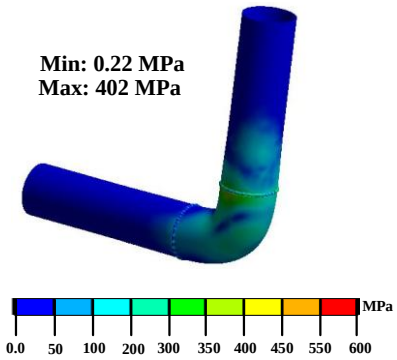
3.2 mm	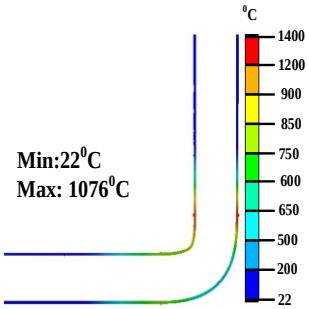	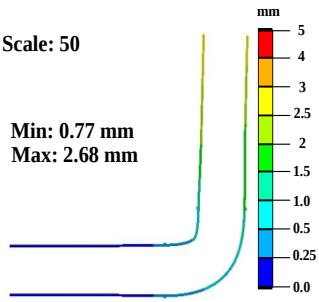	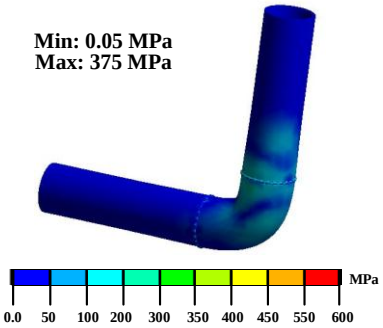
4.0 mm	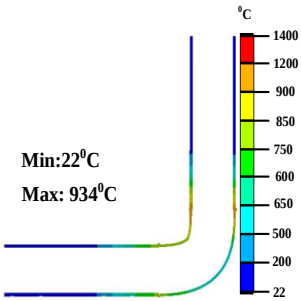	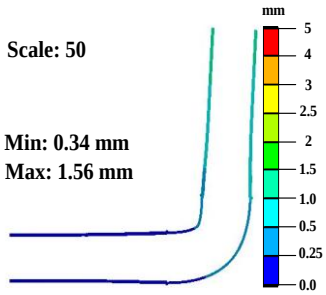	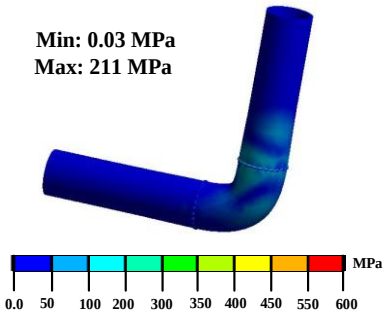
5.2 mm	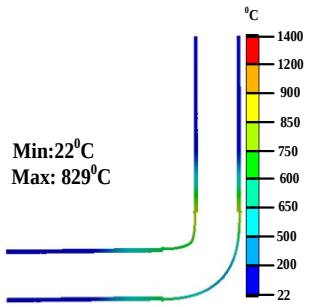	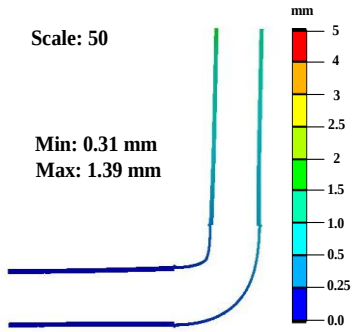	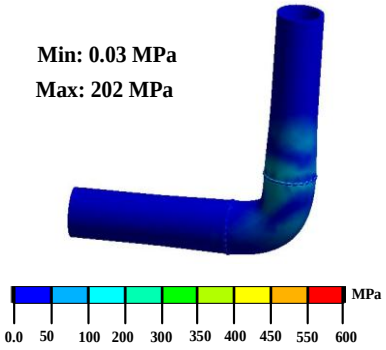

Figure 5. Simulation results at the end of the welding cycle

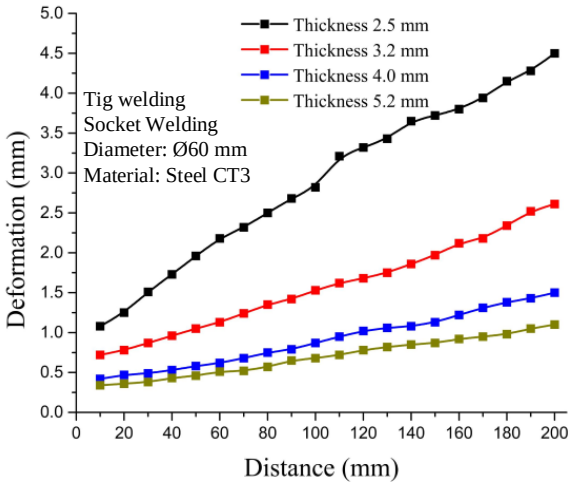

Figure 6. Comparison of pipe deformations for different pipe thicknesses

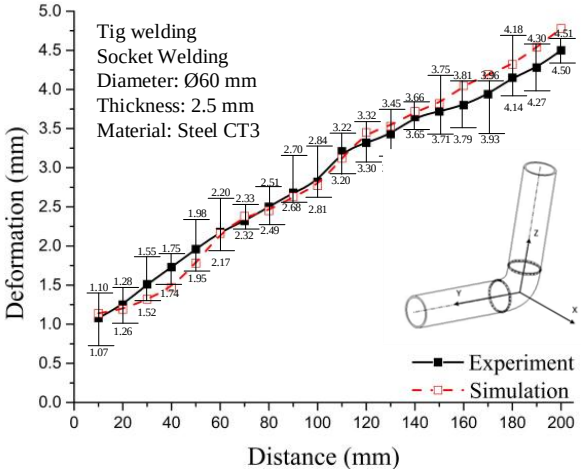

Figure 7. Results for the deformation of the 2.5-mm-thick pipe

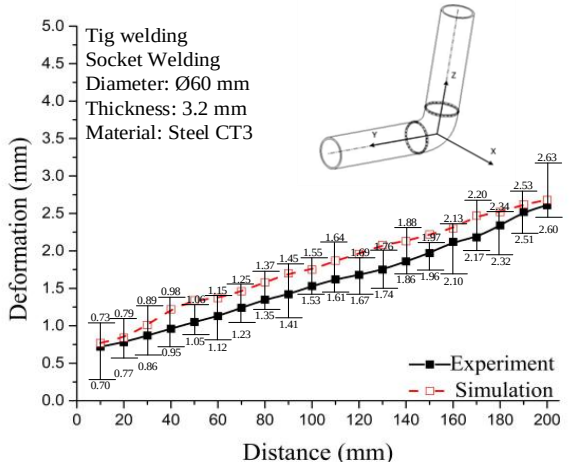

Figure 8. Results for the deformation of the 3.2-mm-thick pipe

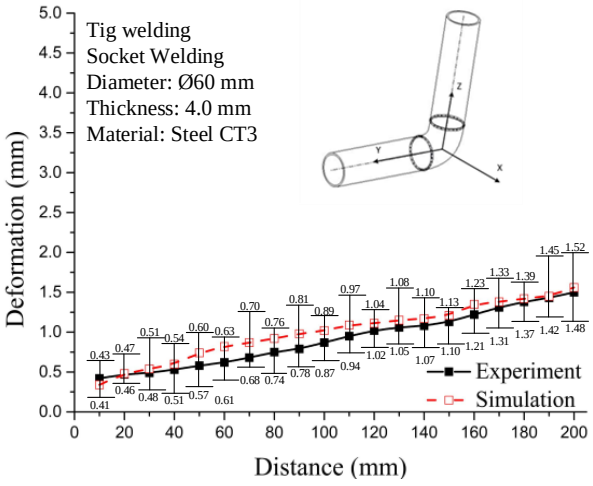

Figure 9. Results for the deformation of the 4.0-mm-thick pipe

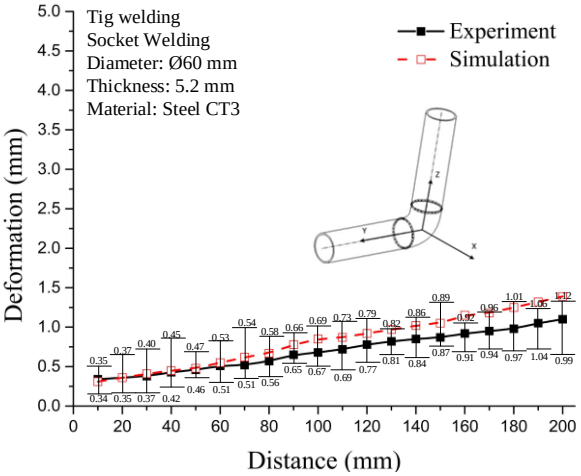

Figure 10. Results for the deformation of the 5.2-mm-thick pipe

To assess simulation accuracy, we performed the welding process experimentally on pipes of four different thicknesses, repeating the process 10 times for each thickness. We then took the average measured deformation and compared it with the simulation results. The experimental deformation results are plotted in Figs. 6–9 alongside the corresponding simulation results (see Tables 5–8 for the data). On the basis of these results, the simulation and experiment agree extremely well. The differences between the simulation and experimental results are due to the heat transfer and conductivity properties of the pipe material. In the simulation, these properties were assumed to be perfect, but in the experiment, they could not function exactly as they did in the simulation. In the experiment, because the heat transfer was slower than that for a perfect material, the pipe temperature at the end of a welding cycle was higher than that in the simulation. This is the main reason for the different deformations between the simulation and experiment.

IV. CONCLUSIONS

In this paper, GMAW was used to weld two pipes joined by a connector. Simulations and experiments were conducted on pipes of four different thicknesses to assess the pipe deformation and residual stress after welding. On the basis of these results, we draw the following conclusions:

- With the same welding parameters, a thinner pipe experiences larger deformation. The largest pipe deformation is located farthest from the welding area.
- The highest stress is in the connector, making it a weak point that must be designed with a higher safety margin.
- The simulation showed how the temperature and stress are distributed. These results explain how the deformation changes with pipe thickness.
- In general, the deformation of the two-pipe welding structure could be predicted by ANSYS simulation using its heat-transfer and structural capabilities.

REFERENCES

[1] Z. Linjie, Z. Jianxun, H. Kalaoui, H. Li, and Y. Wang, A comparative study of the residual deformation of an automotive gear-case assembly due to deep-penetration high-energy welding, Journal of Materials Processing Technology, Vol. 190, pp. 109–116, 2007.

[2] J. Montalvo-Urquizo and Z. Akbay, A. Schmidt, Adaptive finite element models applied to the laser welding problem, Computational Materials Science, Vol. 46, pp. 245–254, 2009.

[3] P. Duranton, J. Devaus, and Robin V., 3D modelling of multipass welding of a 316L stainless steel pipe, Journal of Materials Processing Technology, Vol. 153, pp. 457–463, 2004.

[4] I. Ucok, L. S. Kramer, M. N. Gungor, P. Wolfe, H. Dong, and W. T. Tack, Effect of welding on microstructure and tensile properties of flowformed Ti-6Al-4V tubes, Materials Science and Engineering A, Vol. 410–411, pp. 160–164, 2005.

[5] D. Deng, Y. Zhou, T. Bi, and X. Liu, Experimental and numerical investigations of welding distortion induced by CO2 gas arc welding in thin-plate bead-on joints, Materials and Design, Vol. 52, pp. 720–729, 2013.

[6] H. Hu, J. Liang, Z. Z. Tang, G. Lu, Image correlation method for full-field deformation measurements during metal sheet welding processes, Optik, Vol. 124, pp. 5193–5198, 2013.

[7] S. Murugan, K. Sanjai, B. Rai, and P. V. Kumar, Temperature distribution and residual stresses due to multipass welding in type 304 stainless steel and low carbon steel weld pads, International Journal of Pressure Vessels and Piping, Vol. 78, pp. 307–317, 2001.

[8] H. Bergmann and R. Hilbinger, Numerical simulation of centre line hot cracks in laser beam welding of aluminium close to the sheet edge, Mathematical Modelling of Weld Phenomena, Vol. 695, pp. 658-668, 1998.

[9] J. Goldak, A. Chakravarti, and M. Bibby, A new finite element model for welding heat source, International Journal Metallurgical and Materials Transactions B, Vol. 15, pp. 299-305, 1984.